

Snapshot of sequential SNARE assembling states between membranes shows that N-terminal transient assembly initializes fusion

Yong Jian Wang^a, Feng Li (李峰)^b, Nicolas Rodriguez^c, Xavier Lafosse^d, Christine Gourier^a, Eric Perez^a, and Frederic Pincet^{a,1}

^aLaboratoire de Physique Statistique, École Normale Supérieure, L'université de recherche Paris Sciences et Lettres, CNRS UMR 8550, Sorbonne Universités, Université Pierre-et-Marie-Curie (UPMC) University of Paris 06, Université Paris Diderot, 75005 Paris, France; ^bDepartment of Cell Biology, School of Medicine, Nanobiology Institute, Yale University, West Haven, CT 06516; ^cLaboratoire des Biomolécules, Sorbonne Universités, UPMC University of Paris 06, École Normale Supérieure, Département de Chimie, L'université de recherche Paris Sciences et Lettres, CNRS UMR 7203, 75005 Paris, France; and ^dLaboratoire de Photonique et de Nanostructures, Unité Propre de Recherche 20, CNRS, 91460 Marcoussis, France

Edited by Jacob N. Israelachvili, University of California, Santa Barbara, CA, and approved February 18, 2016 (received for review September 25, 2015)

Many prominent biological processes are driven by protein assembling between membranes. Understanding the mechanisms then entails determining the assembling pathway of the involved proteins. Because the intermediates are by nature transient and located in the intermembrane space, this determination is generally a very difficult, not to say intractable, problem. Here, by designing a setup with sphere/plane geometry, we have been able to freeze one transient state in which the N-terminal domains of SNARE proteins are assembled. A single camera frame is sufficient to obtain the complete probability of this state with the transmembrane distance. We show that it forms when membranes are 20 nm apart and stabilizes by further assembling of the SNAREs at 8 nm. This setup that fixes the intermembrane distance, and thereby the transient states, while optically probing the level of molecular assembly by Förster resonance energy transfer (FRET) can be used to characterize any other transient transmembrane complexes.

SNARE | SFA | transient state | FRET | N-terminal assembly

In biology, many critical protein–protein interactions occur between membrane surfaces. These interactions include cell-to-cell adhesion (1) to form tissues [e.g., cadherins (2, 3)], infection of cells by enveloped viruses (4, 5) (e.g., viral envelope fusion proteins), and secretion when a storage vesicle containing hormones or transmitters (6, 7) fuses with the plasma membrane [this fusion is achieved by soluble *N*-ethylmaleimide–sensitive factor attachment protein receptors (SNAREs) (8)]. In each of these examples, the biological process is thermodynamically coupled and energetically driven by protein folding/assembly. This coupling means that understanding the molecular mechanism requires a complete characterization of the various intermediate transmembrane protein complexes that appear at different intermembrane distances (Fig. 1*A*). Two challenges render this characterization difficult. First, because of the energy landscape, the intermediates are transient. Second, observing in the nanometer-scale gap between two membranes remains a challenge. Several existing experimental approaches provide partial information. X-ray crystallography gives atomic-level images of the proteins after folding (9, 10), providing a framework but not the pathway. With optical tweezers, continuous unfolding of single molecular complexes can be monitored (11, 12) by applying separation forces. The surface forces apparatus (SFA) (13, 14) provides the only possible way to control intermembrane separation rigidly, the main reaction coordinate of this class of folding processes, by fixing the separation between two apposed membranes with subnanometer-level precision, and allows direct measurements of forces (required to unfold the protein) (15–17) (Figs. 1 and 2). With the SFA, a continuous series of folding intermediates can be frozen and their energetics (the energy landscape) determined (15) (Fig. 1*A*).

However, none of these techniques provide the assembling landscape (i.e., a complete view of the various intermediates that naturally occur during protein folding/assembly between membranes).

SNARE protein assembly, which provides the energy for vesicle fusion in intracellular trafficking, is an archetype transmembrane assembly process in which the molecular landscape is strongly correlated with the membrane separation. In the classical case of synaptic fusion, there are two types of SNARE proteins, which include the synaptic vesicle SNARE, synaptobrevin VAMP2 (v-SNARE), and a heterodimer (t-SNARE) made of the pre-synaptic plasma membrane SNARE proteins Syntaxin 1 and SNAP-25. v-SNARE and t-SNARE zipper to form a SNAREpin between the membranes. The efficiency of the fusion process is controlled by subtle molecular details that ensure the right timing and appropriate release of energy at each binding stage. The crystal structure of the SNARE complex (9, 10) shows that SNAREs assemble to form a highly stable coiled-coil made of four parallel helix bundles. Zippering of the coiled-coil proceeds in a stepwise manner, with a half-zipped SNARE complex being one of the intermediate states (11, 18), but the submolecular details of the zippering process between membranes remain unknown. Notably, it is unclear whether the initial intermediate of SNARE assembly requires the binding of their membrane distal N-terminal regions.

In this article, we demonstrate that using an SFA equipped with a visualizing setup to observe Förster resonance energy transfer (FRET), we are able to access the intermediates of protein assembly between membranes. We exemplify this ability by the study of the assembly of SNAREpin and show that the first step toward complete SNARE zippering is the N-terminal

Significance

Membrane fusion is the key step in cellular traffic, which is induced by the assembly of membrane protein, namely SNARE. How the protein assembly induces membrane fusion remains unknown. Answering this question requires knowledge of the assembly intermediates, which cannot be accessed by conventional methods. We developed an instrument not only to freeze a continuous series of intermediates of SNARE assembly but also to monitor the formation of these domains. Here, we demonstrate that the N-terminal assembly is the initializing step prior to fusion.

Author contributions: E.P. and F.P. designed research; Y.J.W., F.L., C.G., and E.P. performed research; Y.J.W., F.L., N.R., X.L., and C.G. contributed new reagents/analytic tools; Y.J.W., F.L., and F.P. analyzed data; and Y.J.W., F.L., E.P., and F.P. wrote the paper.

The authors declare no conflict of interest.

This article is a PNAS Direct Submission.

¹To whom correspondence should be addressed. Email: pincet@lps.ens.fr.

This article contains supporting information online at www.pnas.org/lookup/suppl/doi:10.1073/pnas.1518935113/-DCSupplemental.

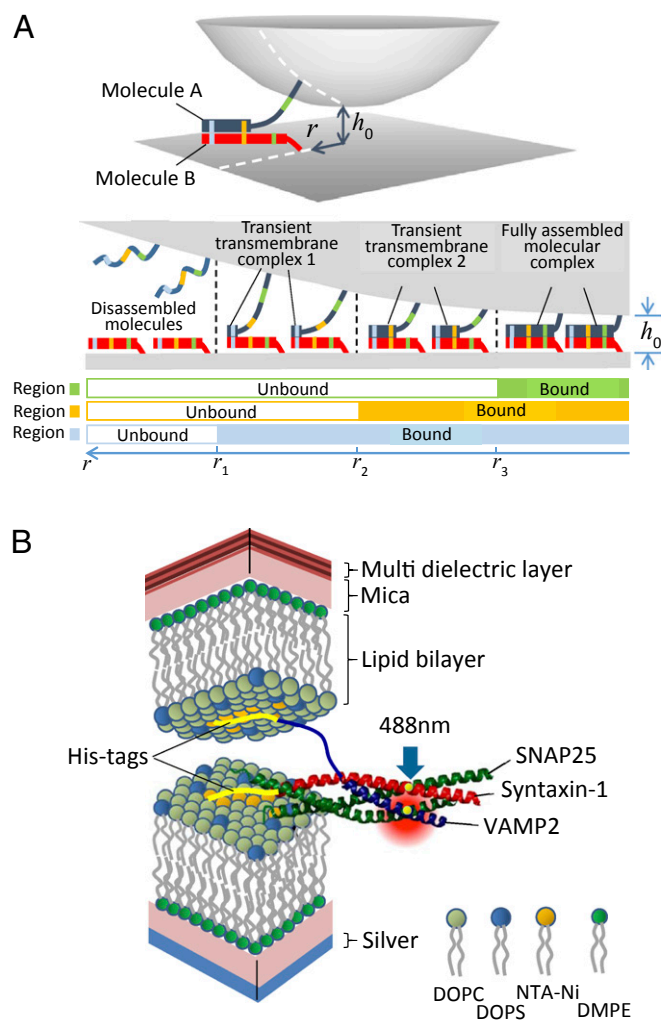


Fig. 1. Transient transmembrane molecular intermediates: how to visualize them. (A, *Upper*) Two molecules assemble to form a molecular complex between a spherical surface and a flat surface, with a fixed closest separation distance, h_0 , at the center. This geometry is the same as the geometry in the FRET/SFA. As the surfaces come closer, the level of assembly of the molecules increases. (A, *Lower*) Cross-section of the *Upper* panel, in which the complex formed by two imaginary molecules, A and B, exhibits four distinct states: disassembled (Left), two intermediate states (Middle), and fully assembled (Right). In the case of the geometry presented here, when the surfaces are covered with molecules A and B, respectively, the level of molecular assembly varies with the distance r to the closest approach on the right-hand side of the diagram because the separation distance increases gradually with r . Hence, at a given r , because the local separation distance is fixed, assembling may only proceed until a certain level; therefore, the two molecules are trapped in an intermediate state. Then, a single snapshot is sufficient to observe all of the intermediate states at various r values, and therefore at all separation distances. In the presented situation, when r is larger than r_1 , molecules A and B are not bound. Between r_1 and r_2 , they are in intermediate state 1; between r_2 and r_3 , intermediate state 2 is reached; and below r_3 , the complex is fully assembled. Considering three regions in molecules A and B, a membrane distal region (blue), a middle region (orange), and a membrane proximal region (green), each state can be fully identified. When none of the regions are bound, the molecules are disassembled. If the blue regions are the only ones bound, the molecular complex is in the transient intermediate state 1. If the blue and orange regions are assembled, but not the green ones, it is in intermediate state 2. When all regions are bound, the complex is fully assembled. (B) SNARE proteins are used to represent molecules A and B. They zipper into a four-helix coiled-coil between the membranes. In vivo, the progression of the zipper brings the two membranes together and drives them to fuse. The cytosolic domains are His-tagged to be bound to NTA-Ni lipids, mimicking the natural transmembrane anchorage. Membranes are deposited on a mica sheet, the other side of which is coated with either silver (*Lower* mica) or a

assembling, and we determine the exact threshold distance, 20 nm, at which this assembling state can occur, before stabilizing at 8 nm.

Results

FRET/SFA. The SFA is a technique that is widely used to measure the force-distance profile between two surfaces that are often functionalized to mimic the surface of a colloidal particle or a biological membrane. The distance between the surfaces is determined with subnanometer accuracy in a spectrometer through the position of fringes of equal chromatic order (FECOs) produced from multiple-beam interferometry with back-silvered mica sheets. The force is measured via the deflection of a spring with a calibrated spring constant. To date, this powerful technique has been used to address a large number of unresolved scientific questions in a wide range of fields [e.g., fundamental physics (19), soft matter physics (20), biology (21)]. It has also been coupled to numerous other techniques, such as friction force measurements (22), electrochemical measurements (23), fluorescence (24, 25), or X-ray diffraction (26). When cognate proteins are anchored on the mica surfaces to study their assembling, the subnanometer-level resolution distance of the SFA gives access to geometrical parameters and to the energy landscape of the assembling (15, 27). However, because of the flexibility of these molecules, the force-distance profile does not allow one to follow the submolecular details that could provide comprehensive information on the intermediate structures: the assembling landscape. To track the formation of molecular complexes, a distance-sensitive phenomenon is required. FRET (28), with its nanometric resolution of the distance between two fluorophores, is an appropriate technique to provide such information. FRET occurs between two fluorophores (29), with the emission spectrum of one (the donor) overlapping the absorption spectrum of the other (the acceptor), and there is energy transfer between the two fluorophores when their separation distance is less than the FRET distance, R_0 , on the order of a few nanometers.

FRET has not been incorporated in an SFA so far. Combining the two techniques into the FRET/SFA is uniquely suited to freeze the absolute distance between two flat membranes, measure the forces, and observe the formation of molecular complexes between the surfaces at the nanometer level (almost the amino acid level for a protein). So, when two molecules (proteins) are labeled, one with a donor and the other with an acceptor, the proximity of the labeled sites (amino acids) on two molecules (proteins) can be estimated in one molecular (protein) complex, and it becomes possible to establish whether molecules (proteins) are assembled at the level of these labeled sites (amino acids).

The FRET/SFA we have designed involves the basic version of the SFA with some modifications (Fig. 2). To allow simultaneous measurement of forces and observation of the FRET signal, the detection of a FRET signal coming from the samples must be made compatible with the interferometric distance measurements. This dual function of the FRET/SFA requires that the mica of the upper lens have high transmittance at the wavelengths of the donor excitation and the acceptor emission and good reflectance of ~ 90 – 95% to observe the FECOs in the other wavelengths. These reflectance/transmittance spectra were made possible by designing an adequate 15-layer multi-dielectric $\text{Ti}_3\text{O}_5/\text{SiO}_2$ coating. The preparation of this special surface is detailed in *Materials and Methods*. The resulting reflectivity spectrum is displayed as the black curve, and the transmission in the SFA setup configuration is displayed in Fig. S1. Second, a band-pass filter is placed at the output of the white light source to transmit only the wavelengths used for the FECOs without interfering with the observation of the FRET signal.

custom-made multi-dielectric layer (*Upper* mica). This setup allows the simultaneous measurement of the intermembrane separation distance by interferometry and the visualization of FRET signal between SNAREs that are labeled with dyes in their N-terminal regions (excitation at 488 nm). The intermembrane distance can be frozen, just as in A, in which case all intermembrane distances can be observed along r .

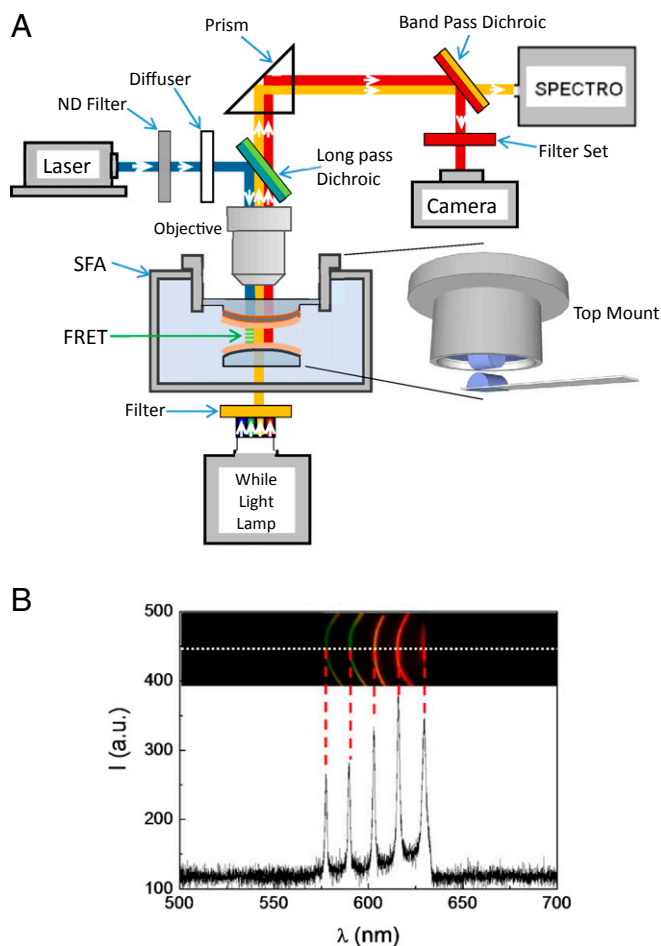


Fig. 2. Diagram of the FRET/SFA setup. (A) Optical pathways for the SFA fringes, fluorescence excitation, and fluorescence emission are denoted by orange, blue, and red lines, respectively. For the SFA, the modified top mount can adapt the optical window with the large diameter. The 30% neutral density (ND) filter is presented in the optical pathway only during the time period of either adjusting the focus or imaging the fluorescently labeled t-SNARE. Magnification of the interacting surfaces is shown in detail in Fig. 1B. (B) Resulting image and spectrum of the FECOs in the spectrometer by this setup. The range of wavelengths used for force measurements (i.e., for observation of the FECOs) is 570–630 nm. A single-line home-made camera with 6,000 pixels captures the spectrum along the white dashed line. The resulting intensities are presented below. Of this range of wavelengths, only fluorescence (or FRET) can pass through the upper multi-dielectric layer presented in Fig. 1B.

Here, we used the Alexa 488 (donor)/Alexa 647 (acceptor) FRET pair. To excite the donor, a 488-nm green laser (Sapphire 488-200 mW; Coherent) is sent to the mica surfaces by means of a long-pass dichroic mirror that reflects the 488-nm light to the sample and that also transmits the donor and acceptor emission wavelengths. If FRET occurs, the fluorescence of the acceptor is emitted from the surfaces, whereas the fluorescence of the donor is decreased. At the optical exit of the SFA, a dichroic band-pass beam splitter reflects the fluorescence emission toward the CCD camera and transmits the FECOs toward the spectrometer. A band-pass filter is placed at the entrance of the CCD camera (RTE/CCD-782-V/HS; Princeton Instruments) to transmit only the wavelengths related to the acceptor or the donor. The power of the laser beam is carefully tuned to prevent photobleaching while capturing the fluorescent image; in the experiments presented here, it was set at 20 mW. The CCD camera is used to capture the fluorescent image. A scheme of the optical setup is presented in Fig. 2A, and the resulting image of the FECOs in the spectrometer is shown in Fig. 2B.

This sensitive system we have developed allows FRET measurements between probes placed at known locations in the proteins folding/assembling between two bilayers, which are brought together (and can be withdrawn) with rigidly controlled separation (Fig. 1B). This rigid control makes it possible to read out the intramolecular separations within assembling complexes at each intermembrane distance. The FRET/SFA can, in parallel, measure forces as in a standard SFA, so that when it is desirable, the assembling and energy landscapes can be directly compared.

SNAREpin Formation Observed with the FRET/SFA. We have used this experimental setup with SNAREs that are labeled at their N-terminal region: t-SNARE with Alexa 488 and v-SNARE with Alexa 647 (Fig. 1B). Labeling is obtained by binding the dyes to a single Cys at the N terminus of each protein (the labeling procedure is described in *SI Materials and Methods*). The necessary mutations of the SNAREs do not affect their ability to fuse membranes (Fig. S2). Our SNAREs also possess a 12× His tag at their C terminus that enables their incorporation in the apposing bilayers containing 10% (mol/mol) lipids with nickel in their polar heads (*Materials and Methods*). The final SNARE density in the membrane is about one protein per 200 lipids. It has been previously shown that lipid-anchoring the SNARE is sufficient to keep the fusion activity (30). When the two SNARE-decorated membranes are brought together and subsequently separated, adhesion is observed (Fig. 3A). This adhesion vanishes in the control experiments, in which t-SNARE is blocked to prevent SNAREpin formation. Simultaneous measurement of the FRET signal when the membranes are contacting shows that SNAREpin forms in the contact area. The FRET signal disappears in the case of the control experiment, indicating that the presence of SNARE complexes is responsible for the observed adhesion (Fig. 3B). We have previously shown that the long-range repulsion in the energy profiles presented in Fig. 3A is directly correlated with the local SNARE density (15). Briefly, when the surfaces are between 10 nm and 20 nm during the approach, the SNAREs are not bound yet, they behave like polymers. The repulsion exponentially decays with the distance, and the prefactor (extrapolated repulsion when the surfaces are in contact) is proportional to the density. Dividing the adhesion energy, $\sim 0.2 \text{ k}_B\text{T}/\text{nm}^2$, where $k_B\text{T}$ is the thermal energy, by the density resulting from this fit directly provides the energy per SNAREpin between the membranes, which is $29 \pm 4 \text{ k}_B\text{T}$. This value is consistent with the value previously measured (15), confirming that SNAREpins form in a specific and normal manner between the membranes and showing that the FRET/SFA is suitable to study the arrangements and interactions of molecular complexes confined between two surfaces.

The FRET images can be analyzed further based on the fact that a continuous series of folding intermediates of SNAREpins are frozen in the SFA. The geometry of the membranes resembles the geometry of a sphere of radius R facing a flat plane (Fig. 1A). Placing the membranes in close proximity (minimum distance h_0) is equivalent to observing simultaneously all separation distances, h , while moving at a distance r away from the contact location (Fig. 1A):

$$h \approx r^2 / (2R) + h_0. \quad [1]$$

Hence, a picture of the FRET signal over the whole area of the membranes directly provides a snapshot of the N-terminal assembly at all distances. The thickness of the cylindrical lens (a few millimeters) imposes that the objective be far from the mica surface. Hence, the FRET signal remains weak. To increase the signal/noise ratio, we spin-averaged each image by successive rotations around the point of closest distance (*Materials and Methods*). The main difficulty is to localize this center of rotation precisely. By testing several positions from the raw FRET signal (Fig. S3C), we estimate that our accuracy, δ , is better than 10 pixels (i.e., better than $3 \mu\text{m}$). The resulting spin-averaged picture is presented in Fig. 4A. The FRET signal profile with the distance

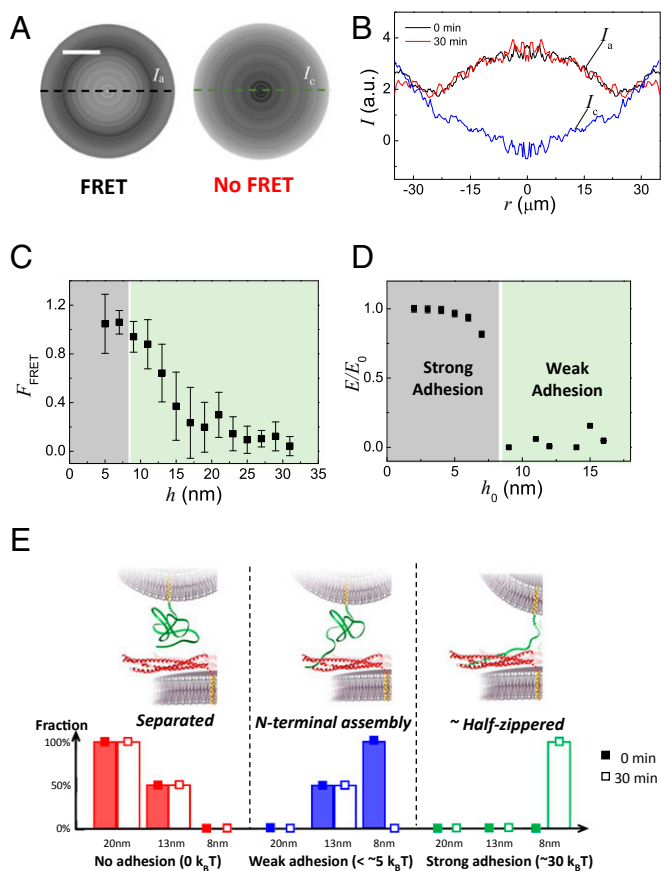


Fig. 4. Stable N-terminal assembly is required for initial binding of the SNAREs. (A, Left) Spin-averaged picture (Materials and Methods and Fig. S3) of the FRET signal between two membranes decorated with fluorescently labeled t-SNARE and v-SNARE, respectively. (A, Right) Spin-averaged picture of the FRET signal in the control experiment. (Scale bar, 20 μm .) (B) Intensities taken along the dashed line through the center to form the intensity profiles are displayed: I_a (black and red lines) represents the intensity of the fluorescently labeled t-SNARE and v-SNARE experiments, whereas I_c (blue) is the control and r equals 0 at the center. The black line shows the intensity right after the contact, and the red line was obtained after the surfaces were kept in contact for 30 min. The two lines are overlapping, revealing no time dependence of the FRET signal. The variations in I_c are due to optical interferences. Hence, the actual FRET signal is the difference between I_a and I_c . (C) Fraction of the N-terminal assembly in the total population of SNARE pairs with the intermembrane separation distance h (obtained from r through Eq. 1). The N-terminal domains are only 100% assembled when $h < 8$ nm. The error bars are the SD, obtained by averaging 20–40 data points in four separate experiments. (D) Adhesion of t-SNARE- and v-SNARE-decorated membranes in the SFA with h_0 , the minimal intermembrane separation reached during the approach/separation cycle, is normalized by the strongest adhesion [same data as in the study by Li et al. (15)]. The membranes were kept at distance h_0 for at least 20 min. (E) Various SNARE complex states in the SFA; their respective energies; and the distribution of these states after 0 and 30 min in contact at $h = 8$ nm, $h = 13$ nm, and $h = 20$ nm. Solid bars represent 0 min, and open bars represent 30 min.

half-zipped state (or possibly zippered beyond). These observations allow us to separate the two situations: upon contact and after 30 min of contact.

First, upon contact, N-terminal regions of the SNARE immediately bind in the low-energy state. Below 8 nm, virtually all SNAREpins are assembled in their N-terminal region. Between 8 nm and 20 nm, only a fraction of them are bound; this fraction decreases as h increases. Beyond 20 nm, no SNAREpins are assembled.

Second, after 30 min, the SNAREpins have transitioned toward the half-zipped state for $h < 8$ nm. Above 8 nm, and because

there is no easily detectable adhesion, the SNAREpins are only in the weak-energy state. These results are summarized in Fig. 4E.

The long delay for the transition toward the half-zipped state indicates a high-activation energy barrier. Assuming a standard density of the transition time, the activation energy can be written as $E_a = k_B T \ln(\nu_0 \tau)$, where ν_0 is the frequency of escape attempt, τ is the characteristic time, and $k_B T$ is the thermal energy. In water, for this type of molecule, ν_0 is between 10^{10} s^{-1} and 10^8 s^{-1} , and $\tau \sim 1,000$ s here. This characteristic time leads to $E_a \sim 25\text{--}30 k_B T$.

These results imply that, in vivo, synaptic vesicles must be brought as close as 20 nm, and preferably 8 nm, from the pre-synaptic plasma membrane to start SNAREpin formation. The long transition time, τ , between the N-terminal weakly bound state and the high-energy half-zipped state suggests that an active mechanism exists to accelerate the transition process, possibly through the use of regulatory factors.

This observation of the first transient state during SNARE zippering between membranes shows the sensitivity and efficiency of the FRET/SFA to detect and characterize intermediate structures between closely apposed membranes. It opens up the way to monitor other transmembrane transient states that cannot be observed otherwise.

Materials and Methods

Chemicals. The lipids used in this study are 1,2-dimyristoyl-*sn*-glycero-3-phosphoethanolamine (DMPE) (850745X), 1,2-dioleoyl-*sn*-glycero-3-phosphocholine (DOPC) (850375C), 1,2-dioleoyl-*sn*-glycero-3-[phospho-L-serine] (sodium salt) (DOPS) (840035C), and 1,2-dioleoyl-*sn*-glycero-3-[(N-(5-amino-1-carboxypentyl)iminodiacetic acid)succinyl] (nickel salt) (NTA-Ni) (79404), which were all purchased from Avanti Polar Lipids. More details on buffers and other chemicals are provided in SI Materials and Methods.

SNARE Proteins. SNARE proteins are illustrated in Fig. S5.

Cytosolic v-SNARE with end-of-sequence 12 \times His (v-SNARE). The v-SNARE for the FRET/SFA study is made of the cytoplasmic domain of mouse VAMP2 (residues 1–96 with a single Cys, S28C, and C-terminal 12 \times His).

Cytosolic t-SNARE with end-of-sequence 12 \times His (t-SNARE). The t-SNARE for the FRET/SFA study is made of the cytoplasmic domain of rat Syntaxin 1A (residues 1–265 with a single Cys, S193C, and C-terminal 12 \times His) and mouse His6-SNAP25 (residues 1–206, Cys-free).

Details on protein constructs, expression, and purification are given in SI Materials and Methods.

Reflective Coating on Mica. The lower mica has the backside surface coated with a 67-nm silver layer prepared by a thermal evaporator in a clean room of class 1,000.

The backside of the upper mica has a custom coating made of 15 or 13 alternating Ti_3O_5 and SiO_2 layers starting with Ti_3O_5 , with a total thickness of 1.1 μm . More precisely, the technique used is an ion-assisted deposition [i.e., E-beam evaporation (MEB 800; Plassys) with ion assistance provided by an ion gun (EH 1000 source; KRI)]. The design, synthesis, and refinement of the custom coating have been done theoretically with Essential MacLeod software. Targets of reflectivity, R , have to be set. In our case, we wanted low R ($\sim 5\%$) for both 488- to 520-nm spectral regions and spectral regions above 660 nm and high R ($\sim 95\%$) for spectral regions between 570 nm and 630 nm. The optimization uses SiO_2 and Ti_3O_5 mean refractive indices for the entire considered spectral range.

From given initial thicknesses to the theoretical stack at an arbitrary wavelength of this range, the algorithm finds solutions with different figures of merit. As an example, for 15 layers, we chose one of these solutions for which the thickness of each layer is (starting from the mica surface) as follows: 65.69 nm (Ti_3O_5)/129.59 nm (SiO_2)/72.65 nm (Ti_3O_5)/35.48 nm (SiO_2)/29.32 nm (Ti_3O_5)/182.25 nm (SiO_2)/66.43 nm (Ti_3O_5)/89.79 nm (SiO_2)/79.51 nm (Ti_3O_5)/111.51 nm (SiO_2)/25.16 nm (Ti_3O_5)/24.02 nm (SiO_2)/136.10 nm (Ti_3O_5)/67.05 nm (SiO_2)/94.86 nm (Ti_3O_5). The deposition is made with the following protocol. Both Ti_3O_5 and SiO_2 are deposited at a rate of 0.25 $\text{nm}\cdot\text{s}^{-1}$. Starting materials are Ti_3O_5 and SiO_2 of 1- to 3-mm pieces put in molybdenum liners. To avoid stress issues on the mica that would curve it, we set the ion gun discharge voltage at 100 V and discharge current at 1 A. The background pressure before adding gases was 1.0×10^{-7} millibars, and the working pressure was $\sim 3.0 \times 10^{-4}$ millibars with flows of 5 standard cubic centimeters per minute (sccm) of Ar and 5 sccm of O_2 for the ion source, and 10 sccm of Ar for the keeper (plasma bridge). The layer thicknesses were followed in real time

using both a quartz microbalance and an ellipsometer (here, we used a 60.5° angle of incidence and 580-nm wavelength).

The reflectivity of the coating is provided in Fig. S1.

SNARE Layer Reconstitution. To prepare the sample for the deposition of the lipid bilayer, the backside-coated mica is glued onto the lens of the SFA by thermal epoxy, with the coated surface contacting the glue. The multi-dielectric-coated mica is glued onto the upper lens, and the silver-coated mica is glued onto the lower lens. Then, the lenses are transferred into water and held vertically in a home-built Langmuir trough. The DMPE chloroform solution is directly used as purchased for the first lipid leaflet on both mica surfaces. For the second leaflet, a mixture of the chloroform solutions of DOPC, DOPS, and NTA-Ni with the lipid molar ratios of 80%, 10%, and 10%, respectively, was used. The mixture has undergone three freeze (by liquid nitrogen) and thaw cycles to homogenize the solution before use. The rest of the procedure is the same as the one we previously reported (15). Details are provided in *SI Materials and Methods*.

In the control experiment that follows a fluorescently labeled t-SNARE and v-SNARE experiment, the lower lens is taken off from the SFA chamber, kept immersed in buffer in a 5-mL beaker, and further incubated with nonlabeled His tag-free v-SNARE (final concentration of 0.2 μM) at 4 °C overnight. It undergoes the same procedure to rinse off unbound protein and is remounted onto the apparatus.

SFA Force Measurement. A homemade SFA similar to the original design (13) is used, except for the modification on the top mount, as shown in Figs. 1B and 2A. It can adapt a large optical window with the SFA lens at the center. This modification increases the angle through which the emission of the acceptor is collected, and therefore improves the optical sensitivity for the FRET signal. The upper lens is initially glued onto an optically smooth polished glass slide, provided by Optique Fichou. This special upper lens is used in the deposition of the lipid bilayer. One band-pass filter (from 570–630 nm) is added in front of the white light source, which limits the wavelength range of the fringes for the FECOs but does not disturb the force measurement. The on/off switching of the white light does not give any difference on the intensity of the dark image captured by the CCD camera at the same exposure time for the fluorescent imaging, which proves that the filtered white light source does not interfere with the fluorescent signal. The characteristic wavelengths of the mercury lamp are used for the calibration of the spectrometer. The procedure of the force measurement is the same as described before (15). The spring constant of the cantilever is precalibrated, and its value is 109 N/m.

Fluorescence Detection. A Genesis MX 488-1000 STM laser purchased from Coherent is used to excite Alexa 488. The laser beam is reflected to the sample by a long-pass dichroic mirror with a cutoff at 500 nm, purchased from Edmunds Optics. Between the laser source and the long-pass dichroic mirror, an engineered 20° diffuser from Thorlabs is used to enlarge the illuminated area on the sample. The total optical power illuminating the sample is only about 400 μW, as measured by a photodetector. A band-pass dichroic beam splitter (transparent from 565–655 nm) from Chroma Technology Corporation is used to reflect the fluorescent light to the CCD camera while letting the 570–630-nm light pass to the spectrometer. In front of the CCD camera (RTE/CCD-782-V/HS; Princeton Instruments), there is a multifilter unit with two band-pass filters, both from Edmunds Optics. The transparent wavelength ranges are from 515–560 nm and from 650–700 nm for the emissions of Alexa 488 and Alexa 647, respectively. The setup of the fluorescent detection is displayed in Fig. 2.

When the separation distance between the samples, controlled by monitoring the fringes, is less than 500 nm, one 30% neutral filter is added in front of the laser before turning on the laser to adjust the focus of the fluorescent image. The focus is adjusted with the observation of the fluorescent image of t-SNARE. The 30% neutral filter is also present to capture fluorescent images of t-SNARE, but not for fluorescent images of v-SNARE. The longest exposure time for each fluorescence image is 5 s to avoid any bleaching effect or saturation of the detector.

Spin-Averaged Image and Intensity Profile. To obtain the spin-averaged image, the initial FRET image (Fig. S3C) is rotated 119 times by 3°. This process produces 120 images, representing the initial image turned by 0°, 3°, 6°, ..., 357°. Then, these 120 images are averaged. The whole process is done by a macro programed in ImageJ (NIH). Intensity profiles, such as the one presented in Fig. 4B, are plots of the intensity values along a straight line across the center of the spin-averaged image. Because the region close to the spin center does not contain many pixels, to perform the average, large fluctuations can be observed. In our system, the data $I_{\text{FRET}}(r)$ of r less than 0.7 μm (two pixels from the center) are not representative of a real average. They should be disregarded for the analysis.

ACKNOWLEDGMENTS. We thank Prof. Jacob Israelachvili (Department of Chemical Engineering, University of California, Santa Barbara), Prof. James Rothman (Yale University), and Prof. Erdem Karatekin (Yale University) for valuable discussions. This work was supported by Agence Nationale de la Recherche Grant ANR-12-BSV5-0002 (to F.P.) and a Fondation Pierre-Gilles de Gennes fellowship (to Y.J.W.).

1. Berrier AL, Yamada KM (2007) Cell-matrix adhesion. *J Cell Physiol* 213(3):565–573.
2. Cavallaro U, Christofori G (2004) Cell adhesion and signalling by cadherins and Ig-CAMs in cancer. *Nat Rev Cancer* 4(2):118–132.
3. Thiery JP (2003) Cell adhesion in development: A complex signaling network. *Curr Opin Genet Dev* 13(4):365–371.
4. White JM, Delos SE, Brecher M, Schornberg K (2008) Structures and mechanisms of viral membrane fusion proteins: Multiple variations on a common theme. *Crit Rev Biochem Mol Biol* 43(3):189–219.
5. Harrison SC (2008) Viral membrane fusion. *Nat Struct Mol Biol* 15(7):690–698.
6. Martens S, McMahon HT (2008) Mechanisms of membrane fusion: Disparate players and common principles. *Nat Rev Mol Cell Biol* 9(7):543–556.
7. Rizo J, Rosenmund C (2008) Synaptic vesicle fusion. *Nat Struct Mol Biol* 15(7):665–674.
8. Weber T, et al. (1998) SNAREpins: Minimal machinery for membrane fusion. *Cell* 92(6):759–772.
9. Poirier MA, et al. (1998) The synaptic SNARE complex is a parallel four-stranded helical bundle. *Nat Struct Mol Biol* 5(9):765–769.
10. Sutton RB, Fasshauer D, Jahn R, Brunger AT (1998) Crystal structure of a SNARE complex involved in synaptic exocytosis at 2.4 Å resolution. *Nature* 395(6700):347–353.
11. Gao Y, et al. (2012) Single reconstituted neuronal SNARE complexes zipper in three distinct stages. *Science* 337(6100):1340–1343.
12. Zorman S, et al. (2014) Common intermediates and kinetics, but different energetics, in the assembly of SNARE proteins. *eLife* 3:e03348.
13. Israelachvili J, Adams G (1978) Measurement of forces between two mica surfaces in aqueous electrolyte solutions in the range 0–100 nm. *J Chem Soc* 1(74):975–1001.
14. Israelachvili J, Marra J (1986) Direct methods for measuring conformational water forces (hydration forces) between membrane and other surfaces. *Methods Enzymol* 127:353–360.
15. Li F, et al. (2007) Energetics and dynamics of SNAREpin folding across lipid bilayers. *Nat Struct Mol Biol* 14(10):890–896.
16. Prakasam AK, Maruthamuthu V, Leckband DE (2006) Similarities between heterophilic and homophilic cadherin adhesion. *Proc Natl Acad Sci USA* 103(42):15434–15439.
17. Li F, et al. (2011) Complexin activates and clamps SNAREpins by a common mechanism involving an intermediate energetic state. *Nat Struct Mol Biol* 18(8):941–946.
18. Li F, et al. (2014) A half-zipped SNARE complex represents a functional intermediate in membrane fusion. *J Am Chem Soc* 136(9):3456–3464.
19. Tabor D, Winterton RH (1968) Surface forces: Direct measurement of normal and retarded van der Waals forces. *Nature* 219(5159):1120–1121.
20. Luckham PF, Klein J (1985) Interactions between smooth solid-surfaces in solutions of adsorbing and nonadsorbing polymers in good solvent conditions. *Macromolecules* 18(4):721–728.
21. Helm CA, Knoll W, Israelachvili JN (1991) Measurement of ligand-receptor interactions. *Proc Natl Acad Sci USA* 88(18):8169–8173.
22. Israelachvili JN, Chen YL, Yoshizawa H (1994) Relationship between adhesion and friction forces. *J Adhes Sci Technol* 8(11):1231–1249.
23. Valtiner M, Banquy X, Kristiansen K, Greene GW, Israelachvili JN (2012) The electrochemical surface forces apparatus: The effect of surface roughness, electrostatic surface potentials, and anodic oxide growth on interaction forces, and friction between dissimilar surfaces in aqueous solutions. *Langmuir* 28(36):13080–13093.
24. Wong JSS, Hong LA, Bae SC, Granick S (2010) Fluorescence recovery after photobleaching measurements of polymers in a surface forces apparatus. *J Polym Sci B Polym Phys* 48(24):2582–2588.
25. Alig ARG, Gourdon D, Israelachvili J (2007) Properties of confined and sheared rhodamine B films studied by SFA-FECO spectroscopy. *J Phys Chem B* 111(1):95–106.
26. Golan Y, et al. (2002) The X-ray surface forces apparatus for simultaneous X-ray diffraction and direct normal and lateral force measurements. *Rev Sci Instrum* 73(6):2486–2488.
27. Perez E, Li F, Taresté D, Pincet F (2008) The surface force apparatus to reveal the energetics of biomolecules assembly. Application to DNA bases pairing and SNARE fusion proteins folding. *Cell Mol Bieng* 14(4):240–246.
28. Stryer L, Haugland RP (1967) Energy transfer: A spectroscopic ruler. *Proc Natl Acad Sci USA* 58(2):719–726.
29. Helms V (2008) *Principles of Computational Cell Biology* (Wiley-Blackwell, Weinheim, Germany).
30. McNew JA, et al. (2000) Close is not enough: SNARE-dependent membrane fusion requires an active mechanism that transduces force to membrane anchors. *J Cell Biol* 150(1):105–117.
31. Melia TJ, et al. (2002) Regulation of membrane fusion by the membrane-proximal coil of the t-SNARE during zippering of SNAREpins. *J Cell Biol* 158(5):929–940.
32. Weninger K, Bowen ME, Choi UB, Chu S, Brunger AT (2008) Accessory proteins stabilize the acceptor complex for synaptobrevin, the 1:1 syntaxin/SNAP-25 complex. *Structure* 16(2):308–320.
33. Xiao W, Poirier MA, Bennett MK, Shin YK (2001) The neuronal t-SNARE complex is a parallel four-helix bundle. *Nat Struct Mol Biol* 8(4):308–311.